

Use of super-Gaussian-Bessel beams in free-space optical interconnect systems

Nedal Al-Ababneh

Jordan University of Science and Technology
Department of Electrical Engineering
P.O. Box 3030
Irbid, 22110, Jordan
E-mail: nedalk@just.edu.jo

Jaser A. Sa'ed

Birzeit University
Department of Electrical Engineering
P.O. Box 14
Birzeit, Palestine

Abstract. The performance of a free-space optical interconnect (FSOI) system based on a super-Gaussian-Bessel (SGB) beam is evaluated. The signal-to-noise ratio (SNR) is used as the performance measure. The SNR of an FSOI system utilizing SGB is analyzed, evaluated, and compared with the SNR of the system that uses a Bessel beam. We show that for large interconnect distance the achievable SNR of the former is superior to that of the latter. © 2008 Society of Photo-Optical Instrumentation Engineers. [DOI: 10.1117/1.2992622]

Subject terms: free-space optical interconnects; nondiffracting beams; bessel beams; super-Gaussian-Bessel-beams; signal to noise ratio.

Paper 080179R received Mar. 6, 2008; revised manuscript received Jul. 13, 2008; accepted for publication Aug. 7, 2008; published online Oct. 14, 2008.

1 Introduction

Board-to-board and chip-to-chip data rates are continuing to increase in most digital computing systems.¹ The increase in individual line rate and bandwidth density drives the need to replace the traditional copper interconnects with optical interconnects that can operate at high data rate while keeping an acceptable level of interconnect performance. One of the most interesting technologies for this purpose is the use of free space optical interconnects (FSOIs).²⁻⁵ Using this technology, a high bandwidth density with parallel data transmission between boards (or chips) can be realized with an array of light sources on one board and a detector array on the receiving board.

Traditionally (FSOI) systems with optical sources that have Gaussian beam profiles have been proposed and analyzed. The diffraction of the Gaussian beams while propagating from source to detector, and the resulting crosstalk, generally impose a trade-off between the SNR and the acceptable propagation distance.^{6,7} To achieve high SNR in a FSOI system with large interconnect length it is necessary to alleviate the effects of diffraction, and to minimize the crosstalk for a given interconnect length.

One interesting concept to reduce the diffraction spread in a FSOI with a large propagation distance is the use of nondiffracting Bessel beams.⁸⁻¹⁰ However, the sidelobes of Bessel beams act as major source of crosstalk, which couples to the neighboring channels and severely limits the SNR and the number of data channels that can be realized. Moreover, the fluctuation of the axial intensity of a Bessel beam with propagation distance represents another problem that reduces the tolerance of FSOIs to misalignment and degrades their performance.¹¹⁻¹³ Nevertheless, the Bessel beam outperforms the conventional Gaussian beam, particularly over larger propagation distances.¹⁰

To reduce the effect of the Bessel beam's sidelobes and the fluctuation of its axial intensity as well, we propose the use of super-Gaussian-Bessel (SGB) beams in FSOIs.¹⁴ We exploit the fact that the SGB beam under some conditions

is the best nondiffracting beam. In fact, the SGB beam has low-level sidelobes compared to those of the Bessel beam and has flat axial intensity over a large propagation distance.¹⁵ By exploiting these two features, a FSOI based on SGB beams with an improved performance level operating at large interconnect distances can be achieved.

In this paper the performance of a FSOI system based on SGB beams is evaluated. The SNR is used as a performance measure. The SNR of such a FSOI is analyzed, evaluated, and compared with that of one using Bessel beams. We show that for large propagation distance the achievable SNR of a FSOI based on SGB beams is superior to that of a FSOI based on Bessel beams. In Sec. 2 the propagation of SGB beams in free space is presented and some propagation features are emphasized. In Sec. 3 the FSOI system using SGB beams is described. The SNR is evaluated in Sec. 4. Numerical simulations and discussion are conducted in Sec. 5. Section 6 concludes the paper.

2 SGB Beam Propagation

Consider a SGB beam propagating in the z direction with an incident field E defined at the plane $z=0$ as¹⁵

$$E(r,0) = f^{SG}(r)J_0(\alpha r), \quad (1)$$

where J_0 is the zero order Bessel function of the first kind, α is the transverse wave number which determines the central lobe width of the Bessel function, $r=(x^2+y^2)^{1/2}$ is the transverse distance in the plane $z=0$, and $f^{SG}(r)$ is the super-Gaussian aperture function and is given by

$$f^{SG}(r) = A \exp[-(r/w)^n], \quad (2)$$

where A is constant, n is the beam order, and w is the width of the super-Gaussian function. This beam can be generated as demonstrated in Ref. 16.

Using Fresnel approximation,¹⁵ the diffraction field $E(\rho,z)$ at a distance z is given by

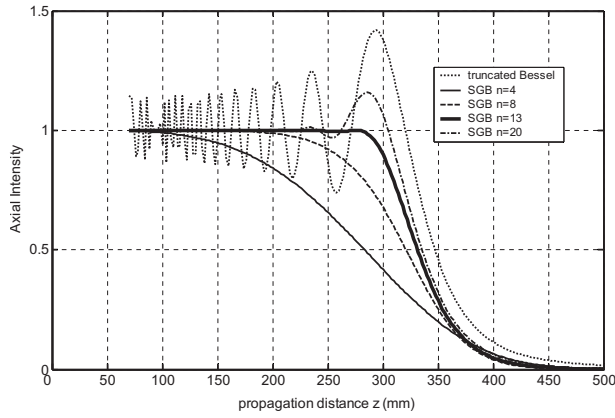


Fig. 1 Axial intensity versus propagation distance.

$$E(\rho, z) = \exp\left(-\frac{ik\rho^2}{2z} - ikz\right) \times \frac{k}{iz} \left[\int_0^\infty E(r, 0) \times J_0\left(\frac{kr\rho}{z}\right) \exp\left(-\frac{ikr^2}{2z}\right) r dr \right], \quad (3)$$

where $k=2\pi/\lambda$ is the wave number, λ is the wavelength, and ρ is the transverse distance in the z plane. The beam intensity $I(\rho, z)$ of the diffraction field is

$$I(\rho, z) = |E(\rho, z)|^2 = \left| \frac{k}{z} \int_0^\infty E(r, 0) \times J_0\left(\frac{kr\rho}{z}\right) \times \exp\left(-\frac{ikr^2}{2z}\right) r dr \right|^2. \quad (4)$$

When $\rho=0$, the axial intensity $I(0, z)$ can be obtained as

$$I(0, z) = \left| \frac{k}{z} \int_0^\infty E(r, 0) \exp\left(-\frac{ikr^2}{2z}\right) r dr \right|^2. \quad (5)$$

At this point two features of SGB beams should be explained. The first feature can be discussed with the aid of Fig. 1. The figure shows the axial intensity of a SGB beam with $A=1$, $w=2$ mm, $\alpha=40$ mm⁻¹ and $\lambda=850$ nm for $n=4, 8, 13$, and 20 . It is noted from the figure that the axial intensity is constant over some propagation distance for a beam of order 13. This means that a flat axial intensity without fluctuation for the SGB beam can be obtained with some optimal beam parameters (beam width, beam order) over a certain propagation distance. We have also plotted on the same figure the axial intensity of a truncated (hard hole with 2-mm radius) Bessel beam for comparison. It is clear from the figure that the axial intensity of the truncated Bessel beam fluctuates with increasing propagation distance.

The second interesting feature of SGB beams is that the sidelobes have lower values than those of a truncated Bessel beam. Figure 2 shows the transverse intensity profiles for both the truncated Bessel beam (hard hole with 2-mm radius) and the SGB beams with beam order 13. It is clear from the figure that the sidelobes of the Bessel beam,

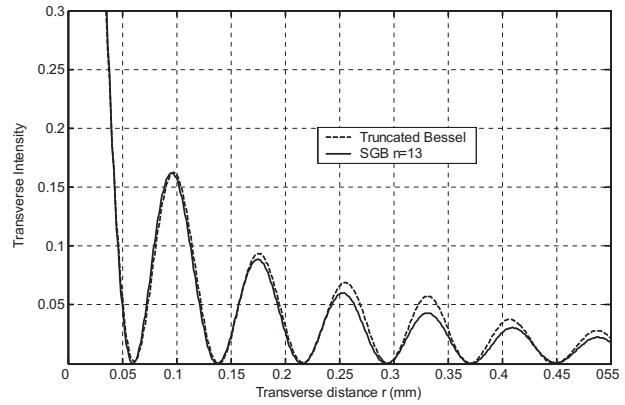


Fig. 2 Transverse intensity versus transverse distance for truncated Bessel and SGB beams.

as represented by the dashed line, have higher values than those of SGB, as represented by the solid line.

The existence of these two features of the SGB beam has motivated us to investigate the use of SGB beams for FSOIs. Because the SGB beam propagates over some distance without oscillations in the axial intensity, the tolerance of the FSOI system to axial misalignment will be higher than that of a FSOI system based on Bessel beams. Moreover, the sidelobes, which represent a major source of noise in a FSOI, cause reduction of the SNR, which represents a figure of merit in a FSOI. In the next section we evaluate the SNR for use as an indicative measure of the usefulness of SGB beams in FSOI systems.

3 SGB-Beam-Based FSOI System

A 2-D representation of a FSOI system using SGB beams is shown in Fig. 3(a). As shown in the figure, an array of light sources is placed in the plane $z=0$. The output beam from each source is assumed to be SGB with radiant beam intensity as given by

$$I(r, z=0) = |A \exp[-(r/w)^n] \times J_0(ar)|^2, \quad (6)$$

where r is the transverse distance in the source array plane. Since finite aperture optical elements are always present in any practical realization, a more realistic model for the

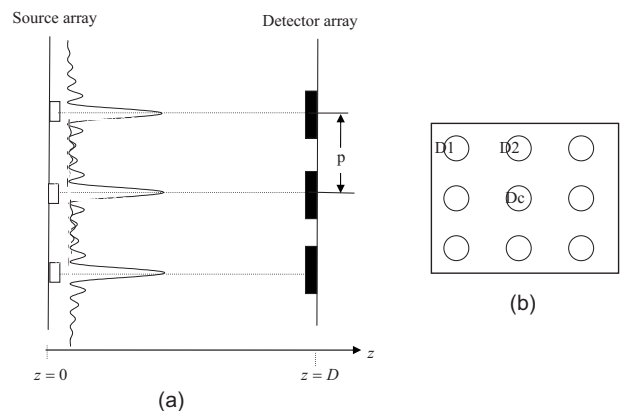


Fig. 3 (a) Simple representation for FSOI system with SGB beam; (b) 2-D representation for detector array.

SGB beam is to assume its presence over just a finite aperture a .

These beams propagate through free space to a detector array located in the plane $z=D$; the beam intensity at the detector array can be found as

$$I(\rho, z = D) = \left| \frac{k}{D} \int_0^a A \exp[-(r/w)^n] \times J_0(\alpha r) J_0\left(\frac{kr\rho}{D}\right) \times \exp\left(-\frac{ikr^2}{2D}\right) r dr \right|^2, \quad (7)$$

where ρ is the transverse distance in the plane of the detector array. Careful examination of Eq. (7) reveals that the irradiance intensity of SGB at the detector plane depends on many parameters, including beam order, beam width, aperture of the super-Gaussian function, central width of the Bessel beam, and optical source aperture. This in turn means that the optical intensity that is coupled to the neighbor detectors also depends on these parameters and that the choice of these parameters must be such that the desired performance level is achieved at a given interconnect distance. In the next section the SNR, which is used as the performance measure, is analyzed, and its dependence on different system parameters is considered.

4 SNR of SGB-Beam-Based FSOI System

To be able to understand the advantages of using SGB beams in FSOI systems, we use the SNR as a performance measure. The SNR in a FSOI can be defined as

$$\text{SNR} = \frac{P_0 \eta}{P_0 \delta + N_{\text{th}}}, \quad (8)$$

where η, δ ($\eta + \delta \leq 1$) represent the fractions of the transmitted beam received by the intended photodetector and by the other photodetectors, respectively, P_0 is the power in each transmitted beam, and N_{th} is the thermal noise and is given by

$$N_{\text{th}} = \text{NEP} \times \sqrt{f}. \quad (9)$$

Here NEP is the noise equivalent power, which is a measure of the photodetector's sensitivity and reflects the amount of the optical power required to achieve a SNR of unity, and f is the channel bandwidth. It is important to note that the numerator of Eq. (8) represents the optical signal power, and the first term in the denominator represents the noise that is due to optical crosstalk. To determine η we refer to Fig. 3(b) and assume that the active channel corresponds to the central detector. In this case η is the fractional amount of power captured by central detector and can be determined by integrating the normalized version of Eq. (7) over the area of the central detector:

$$\begin{aligned} \eta &= \iint_{D_c} I_n(\rho, \theta, z = D) \rho d\rho d\theta \\ &= \int_0^{2\pi} \int_0^d I_n(\rho, \theta, z = D) \rho d\rho d\theta, \end{aligned} \quad (10)$$

where d is the photodetector radius and

$$I_n(\rho, \theta, z = D) = \frac{I(\rho, \theta, z = D)}{\iint_a I(\rho, \theta, z = D)}. \quad (11)$$

Similarly, δ can be found by integrating the normalized light intensity over the area of the other eight neighbor detectors as shown in Fig. 3(b) (excluding the central detector):

$$\begin{aligned} \delta &= \iint_{\text{other det.}} I_n(\rho, \theta, z = D) \rho d\rho d\theta = 4 \iint_{D_1} I_n(\rho, \theta, z \\ &= D) \rho d\rho d\theta + 4 \iint_{D_2} I_n(\rho, \theta, z = D) \rho d\rho d\theta \\ &= 4 \int_0^{2\pi} \int_p^{p+d} I_n(\rho, \theta, z = D) \rho d\rho d\theta \\ &+ 4 \int_0^{2\pi} \int_{\sqrt{2}p}^{\sqrt{2}p+d} I_n(\rho, \theta, z = D) \rho d\rho d\theta, \end{aligned} \quad (12)$$

where p is the center-to-center distance between the detectors. By careful examination of Eqs. (11) and (12) we can note that both η and δ depend on the interconnect distance D , the detector radius d , and the parameters of the SGB beam. Moreover, δ , which represents the crosstalk noise, depends on the distance p between detectors. For a given application the interconnect distance and the detector spacing (channel density) are given and are not used as design parameters. The detector size can be chosen according to the width of the central lobe of the SGB beam for this lobe carries the useful optical signal (information). We also should be careful about the bandwidth of the optical receiver when choosing the detector size, which plays an important role in determining the bandwidth. The design of the FSOI can then be optimized using SGB beam parameters such as beam width and beam order as design parameters. In the next section the optimum choice of these parameters is discussed and the advantage of the using SGB beams is explained.

5 Simulation Analysis and discussion

In this section we consider a FSOI system in which the interconnect distance and the channel (detector) spacing are prespecified. The channel spacing is set to 2.5 mm which corresponds to a channel density of 30 cm⁻². The choice of channel spacing is primarily determined by the size of the aperture of optical source used in the FSOI system. For the SGB beam the following parameters are assumed: wavelength $\lambda=850$ nm, power $P_0=200$ μ W. The individual channel bandwidth is $f=1$ GHz. The noise-equivalent

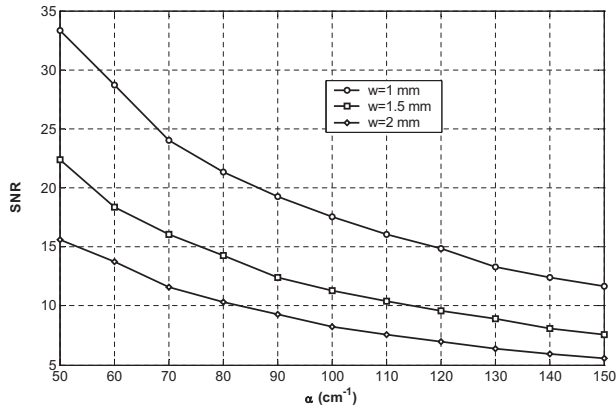


Fig. 4 SNR versus α with super-Gaussian aperture function width as a parameter.

power at the receiver is $NEP=10 \times 10^{-10} \text{ W/Hz}^{1/2}$. The detector size is chosen such that the detector radius d is equal to the half of central lobe width.

Figure 4 shows the SNR versus the (central lobe width) α with the width w of the super-Gaussian aperture function as a parameter. The beam order n for each value of α is chosen such that maximum propagation distance before diffraction can be achieved. It is clear from the figure that high values for SNR can be achieved for specific values for α and the super-Gaussian aperture function width. For example, a SNR higher than 10 can be achieved with $w = 1.5 \text{ mm}$ and $\alpha \leq 110 \text{ cm}^{-1}$ or $w = 2 \text{ mm}$ and $\alpha \leq 80 \text{ cm}^{-1}$. We also note that as α increases, the SNR decreases. In fact, as α increases, the width of the central lobe decreases, which results in a decrease in the received optical signal power and an increase in the crosstalk for a beam of constant power. Moreover, the SNR increases as w decreases for a fixed value of α . This can be explained based on the fact that as the aperture width decreases, the sidelobes decrease while the central lobe remains unaffected, which in turn results in an increase in SNR. At this point it is important to mention that the value of SNR in Fig. 4 for each choice of α and w is obtained using the optimum beam order that gives the highest propagation distance before diffraction occurs. Figure 5 shows the optimum beam order versus α . For a given w the optimum beam order

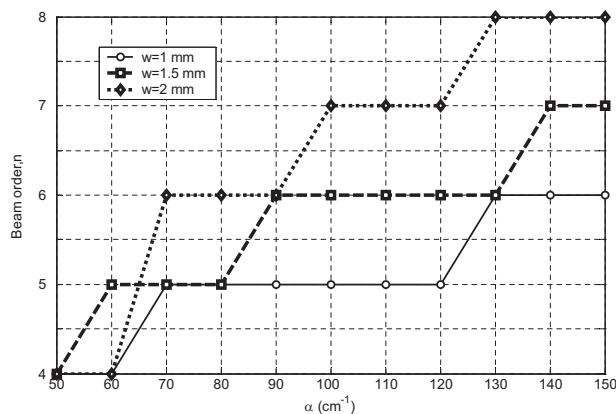


Fig. 5 Optimum beam order versus α with w as a parameter.

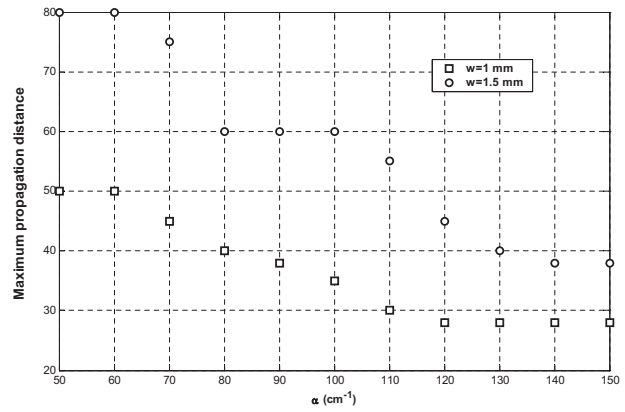


Fig. 6 Maximum propagation distance (cm) versus α with w as a parameter.

increases with α . For $w = 1.5 \text{ mm}$ the required beam order is 6 to achieve a SNR of 10 ($\alpha = 110 \text{ cm}^{-1}$), and the beam order drops to 4 at $\alpha = 80 \text{ cm}^{-1}$ to achieve the same SNR. In fact, the increase in the beam order is required to decrease the crosstalk noise to partially balance the decrease in the signal power as α increases. However, the SNR decreases with increasing α (Fig. 4), which implies that the reduction in the signal power overwhelms the reduction in the noise power resulting from the increased beam order. We also note that for a given α the optimum beam order increases with w . For example, at $\alpha = 110 \text{ cm}^{-1}$ the beam order jumps from 6 to 7 as w changes from $w = 1.5$ to 2 mm . As w increases, the reduction of the sidelobes decreases and a large beam order is required to compensate for this reduction. Again the effect of increasing w overwhelms that of increasing the beam order. In Fig. 6 the maximum propagation distance is plotted against α for two different aperture widths. A large interconnect distance with an acceptable SNR can be achieved using a SGB beam. For $\alpha = 110 \text{ cm}^{-1}$ and $w = 1.5 \text{ mm}$ an interconnect of 55-cm length operating at a SNR of 10 can be realized. To appreciate the advantage of using SGB beams, a performance comparison with that of Bessel Beam is conducted. Figure 7 shows the SNR versus detector radius for three different values of α using the same other parameters used for the

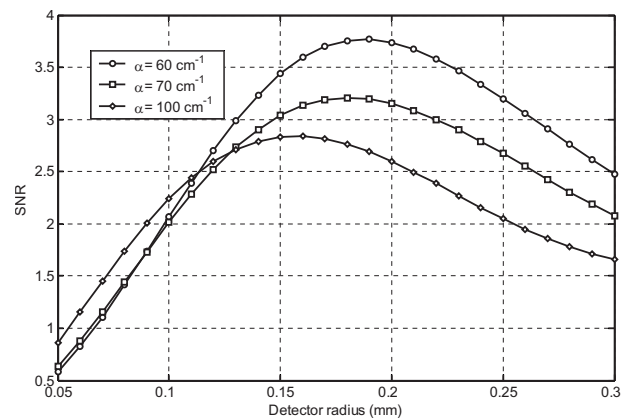


Fig. 7 SNR versus detector radius with α as a parameter for a FSO with Bessel beams.

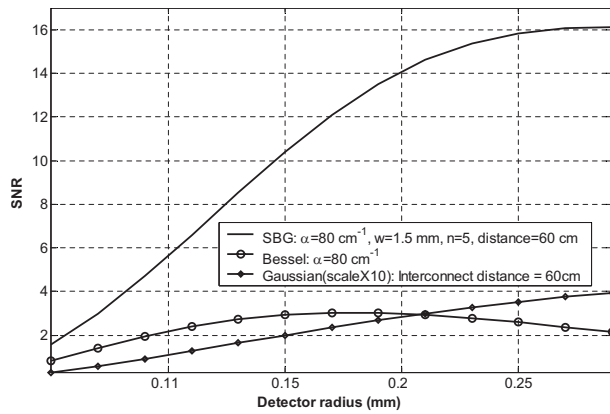


Fig. 8 SNR versus detector radius for SGB, Bessel, and Gaussian beams.

SGB beam system. It is clear from the figure that the optimum values for the SNR are low compared with those of the SGB beam. However, the FSOI using the Bessel beam outperforms that using the conventional Gaussian beam for large propagation distance.⁸ In Fig. 8 the SNR for the Gaussian, Bessel, and SGB beams is plotted as a function of the detector radius. The parameters used for this plot are chosen such the interconnect distance is 60 cm. From the figure we observe that a peak SNR of 15 can be achieved using the SGB beam, while the peak SNRs for the Bessel and Gaussian beams are 3 and 0.4, respectively.

6 Conclusion

We propose the use of SGB beams in long-distance FSOIs. We used the SNR as a performance measure to decide the usefulness of such beams. Our results showed that high values for the SNR can be obtained using SGB beams. We used the beam width and the beam order as design parameters. Our analyses showed that these two parameters, whose values determine the propagation features of the beam, can be used to optimize the design of a FSOI system for maximum SNR. We also included results for a FSOI system based on Bessel and Gaussian beams. The SNRs obtained are low compared with that obtained for the SGB beam system.

References

1. Y. Yadin and M. Orenstein, "Parallel optical interconnects over multimode waveguides using mutually coherent channels and direct detection," *J. Lightwave Technol.* **25**, 3126–3131 (2007).
2. C. J. Henderson, D. G. Leyva, and T. D. Wilkinson, "Free space adaptive optical interconnect at 1.25 Gb/s, with beam steering using

- a ferroelectric liquid-crystal SLM," *J. Lightwave Technol.* **24**, 1989–1997 (2006).
3. M. Gruber, J. Jahns, E. M. ElJoudi, and S. Sinzinger, "Practical realization of massively parallel fiber-free-space optical interconnects," *Appl. Opt.* **40**, 2902–2908 (2001).
4. A. G. Kirk, D. V. Plant, M. H. Ayliffe, M. Chateauf, and F. Lacroix, "Design rules for highly parallel free-space optical interconnects," *IEEE J. Sel. Top. Quantum Electron.* **9**(2), 531–547 (2003).
5. R. Wang, A. D. Rakic, and M. L. Majewski, "Analysis of lensless free-space optical interconnects based on multi-transverse mode vertical-cavity-surface-emitting lasers," *Opt. Commun.* **167**, 261–271 (1999).
6. T. Kurokawa, S. Masto, T. Nakahara, K. Tateno, Y. Ohiso, A. Wakatsuki, and H. Tsuda, "Design approaches for VCSELs and VCSEL-based smart pixels toward parallel optoelectronic processing systems," *Appl. Opt.* **37**, 194–204 (1998).
7. S. Tang, R. T. Chen, L. Garrett, D. Gerold, and M. M. Li, "Design limitations of highly parallel free-space optical interconnects based on arrays of vertical cavity surface-emitting laser diodes, micro-lenses, and photo-detectors," *J. Lightwave Technol.* **12**, 1971–1975 (1994).
8. N. Al-Ababneh, and M. Testorf, "Analysis of free space optical interconnects based on non-diffracting beams," *Opt. Commun.* **242**, 393–400 (2004).
9. C. Yu, M. R. Wang, A. J. Varela, and B. Chen, "High-density non-diffracting beam array for optical interconnection," *Opt. Commun.* **177**, 369–376 (2000).
10. R. P. Macdonald, S. A. Boothroyd, T. Okamoto, J. Chrotowski, and B. A. Syrett, "Inter-board optical link data distribution by Bessel beam shadowing," *Opt. Commun.* **122**, 169–177 (1996).
11. N. Al-Ababneh, "Misalignment analysis of lensless free space optical interconnects," *Opt. Eng.* **45**, 065401-1–065401-8 (2006).
12. D. T. Neilson, "Tolerance of optical interconnections to misalignment," *Appl. Opt.* **38**, 2282–2290 (1999).
13. N. S. F. Ozkan, W. L. Hendrick, P. J. Marchand, and S. C. Esner, "Misalignment tolerance of free-space optical interconnects via statistical methods," *Appl. Opt.* **41**(14), 2686–2694 (2002).
14. J. R. Salazar, G. H. C. New, and S. C. Cerda, "Bessel-Gauss beam optical resonator," *Opt. Commun.* **190**, 117–122 (2001).
15. Z. Jiang, "Super-Gaussian-Bessel beam," *Opt. Commun.* **125**, 207–210 (1996).
16. J. R. Salazar, G. H. C. New, and H. C. Cerda, "Bessel-Gauss beam Optical resonator," *Opt. Commun.* **190**, 117–122 (2001).



Nedal Al-Ababneh received his BSc and MSc degrees in electrical engineering from Jordan University of Science and Technology in 1993 and 1996, respectively. He received his Doctor of engineering degree in Electrical engineering from University of Massachusetts–Lowell (USA) in 2004. He is currently an assistant professor in the Department of Electrical Engineering at Jordan University of Science and Technology. His research interests are in free-space optical interconnects and distributed detection systems.

Jaser A. Sa'ed received his BSc degree in electrical engineering from Birzeit University in 2005. He received his MSc degree in electrical engineering from Jordan University of Science and Technology in 2007. He is an currently instructor in the Department of Electrical engineering at Birzeit University. His research interests are in free-space optical interconnects and digital signal processing.